ISSN 1674-1056
http://cpb.iphy.ac.cn
http://iopscience.iop.org/cpb
中国物理 B
Chinese Physics
中国物理 Chinese Physics B

# Quantum information processing with nitrogen-vacancy centers in diamond

Gang-Qin Liu(刘刚钦)[1,2], Xin-Yu Pan(潘新宇)[1,3,4]
**Citation:**Chin. Phys. B . 2018, 27(2): 020304. **doi:** 10.1088/1674-1056/27/2/020304

Journal homepage: http://cpb.iphy.ac.cn; http://iopscience.iop.org/cpb

**What follows is a list of articles you may be interested in**

---

## Probabilistic direct counterfactual quantum communication

Sheng Zhang(张盛)
Chin. Phys. B . 2017, 26(2): 020304. **doi:** 10.1088/1674-1056/26/2/020304

## Creating nitrogen–vacancy ensembles in diamond for coupling with flux qubit

Ya-Rui Zheng(郑亚锐), Jian Xing(邢健), Yan-Chun Chang(常彦春), Zhi-Guang Yan(闫智广), Hui Deng(邓辉), Yu-Lin Wu(吴玉林), Li Lü(吕力), Xin-Yu Pan(潘新宇), Xiao-Bo Zhu(朱晓波), Dong-Ning Zheng(郑东宁)
Chin. Phys. B . 2017, 26(2): 020305. **doi:** 10.1088/1674-1056/26/2/020305

## Fidelity between Gaussian mixed states with quantum state quadrature variances

Hai-Long Zhang(张海龙), Chun Zhou(周淳), Jian-Hong Shi(史建红), Wan-Su Bao(鲍皖苏)
Chin. Phys. B . 2016, 25(4): 040304. **doi:** 10.1088/1674-1056/25/4/040304

## Time-bin-encoding-based remote states generation of nitrogen-vacancy centers through noisy channels

Su Shi-Lei, Chen Li, Guo Qi, Wang Hong-Fu, Zhu Ai-Dong, Zhang Shou
Chin. Phys. B . 2015, 24(2): 020305. **doi:** 10.1088/1674-1056/24/2/020305

## Implementation of a nonlocal *N*-qubit conditional phase gate using the nitrogen-vacancy center and microtoroidal resonator coupled systems

Cao Cong, Liu Gang, Zhang Ru, Wang Chuan
Chin. Phys. B . 2014, 23(4): 040304. **doi:** 10.1088/1674-1056/23/4/040304

---

TOPICAL REVIEW — Solid-state quantum information processing

# Quantum information processing with nitrogen–vacancy centers in diamond*

Gang-Qin Liu(刘刚钦)[1,2,†] and Xin-Yu Pan(潘新宇)[1,3,4,‡]

[1] Beijing National Laboratory for Condensed Matter Physics, Institute of Physics, Chinese Academy of Sciences (CAS), Beijing 100190, China
[2] Department of Physics, The Chinese University of Hong Kong, Shatin, New Territories, Hong Kong, China
[3] Collaborative Innovation Center of Quantum Matter, Beijing 100871, China
[4] CAS Center of Excellence in Topological Quantum Computation, Beijing 100190, China

(Received 8 September 2017; revised manuscript received 14 December 2017; published online 29 January 2018)

Nitrogen–vacancy (NV) center in diamond is one of the most promising candidates to implement room temperature quantum computing. In this review, we briefly discuss the working principles and recent experimental progresses of this spin qubit. These results focus on understanding and prolonging center spin coherence, steering and probing spin states with dedicated quantum control techniques, and exploiting the quantum nature of these multi-spin systems, such as superposition and entanglement, to demonstrate the superiority of quantum information processing. Those techniques also stimulate the fast development of NV-based quantum sensing, which is an interdisciplinary field with great potential applications.

**Keywords:** nitrogen–vacancy center, quantum information processing, spin coherence, quantum gate

**PACS:** 03.67.Lx, 03.65.Yz, 61.72.jn, 76.70.Hb **DOI:** 10.1088/1674-1056/27/2/020304

## 1. Introduction

Nitrogen–vacancy (NV) center is one of the hundreds color centers in diamond.[1] As shown in Fig. 1(a), it is formed by a substitutional nitrogen atom and an adjacent vacancy in the diamond lattice. Due to its superb spin coherence and optical properties, NV center becomes one of the most promising systems to implement quantum computing at room temperature. In 1997, individual NV center was selectively addressed by Jörg Wrachtrup and coauthors with laser scanning confocal optical microscopy.[2] They also demonstrated that these *single* spins can be polarized, manipulated, and readout with a technique named ODMR (optically detected magnetic resonance). This triggers a large amount of studies in the fields of both quantum computing and quantum sensing, and now NV center still stands at the cutting edge of these fields.

There are a series of theoretical and experimental works toward the quantum information process with NV centers in diamond. These fundamental topics include understanding the spin dynamics[3–12] and charge dynamics,[13–16] preserving center spin coherence by employing isotopic purified diamond[17,18] or dedicate quantum control techniques such as dynamical decoupling[6,19] and dynamical nuclear spin polarization.[20,21] With nearby nuclear spins, quantum registers[22–24] and multiparticle entanglement[25] have been demonstrated. And high-fidelity projective (single-shot) readout of individual spins,[26–29] universal quantum gates[30–35] have developed, which leads to the recent experimental demonstration of quantum error correction,[36,37] entanglement distillation,[38] and quantum algorithms[31,39–42] in this solid-state system. Meanwhile, using NV electron spin as a quantum probe has been proposed and demonstrated,[43,44] which now is at the core of the fast-developing field of quantum sensing.[45]

There are several nice reviews about the basic of NV center[46–49] and the emergent field of diamond quantum sensing.[45,50–54] In this review, we focus on the working principles and recent experimental progresses of NV-based quantum computing, which includes a brief introduction to the ODMR techniques, followed by the understanding and prolonging of center spin coherence, then the physics and techniques to build universal quantum gates, and principal applications of those few spins. Several protocols of scaling up NV-based qubits are discussed at the end of the review.

## 2. Coherent manipulation of single spins

We first introduce the basic spin and optical properties of NV centers in diamond. A six-electron model has been generally accepted to explain the energy levels of the negatively charged $NV^-$ center.[48] As shown in Fig. 1(b), this spin-1 system has ground states of an $^3A$ spin triplet, with a zero-field splitting 2.87 GHz between the $m_S = 0$ and $m_S = \pm 1$ sub-levels. The degeneracy between the $m_S = \pm 1$ states can

*Project supported by the National Basic Research Program of China (Grant Nos. 2014CB921402 and 2015CB921103), the Strategic Priority Research Program of the Chinese Academy of Sciences (Grant No. XDB07010300), the National Natural Science Foundation of China (Grant No. 11574386), and the Key Research Program of the Chinese Academy of Sciences (Grant No. XDPB0803).

†Corresponding author. E-mail: xypan@aphy.iphy.ac.cn
‡Corresponding author. E-mail: gangqinliu@gmail.com

© 2018 Chinese Physical Society and IOP Publishing Ltd 

be lifted by an external magnetic field, as shown in Fig. 1(c), then either one of them together with the $m_S = 0$ state can form a well-defined two-level system, which is the physical realization of a quantum bit (qubit). The quantum state of this spin qubit can be manipulated with resonant microwave (MW) pulses.

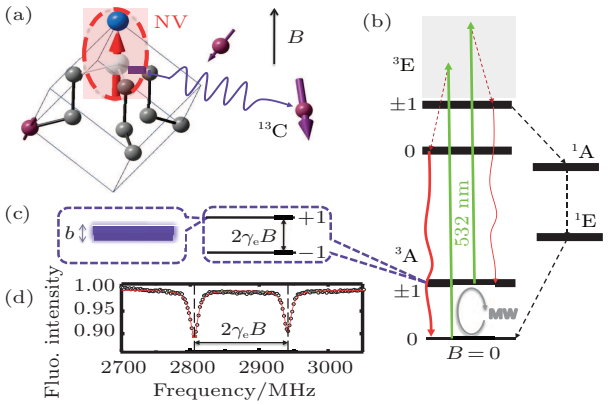



**Fig. 1.** (color online) Nitrogen–vacancy (NV) centers in diamond. (a) An NV center is formed by a substitutional nitrogen atom and an adjacent vacancy in the diamond lattice. (b) The energy levels and optical transitions of the NV electron spin. The spin states can be polarized with green laser and readout by fluorescence intensity. (c) Ground states of an NV center under an external magnetic field $\boldsymbol{B}$. The degeneration of $m_S = \pm 1$ states are lifted by Zeeman effect. The hyperfine interaction with surrounding $^{13}$C nuclear spins brings an inhomogeneous broadening. (d) Typical optical detected magnetic resonance (ODMR) spectrum of an NV center. The strength of the external magnetic field can be extract from the resonant positions of the ODMR spectrum.

The polarization and readout of this qubit is realized by exploiting the spin-dependent optical transitions of NV centers. As shown in Fig. 1(b), the energy gap between the ground $^3$A state and the excited $^3$E state is 1.945 eV (637 nm). A laser pulse with photon energy larger than 1.945 eV (e.g., 532-nm green laser) can excite the electron spin to its excited states, then there is a difference in choosing the paths back to the ground states: the $m_S = \pm 1$ states are more likely to be trapped by the $^1$A singlet and have less fluorescence compared to the $m_S = 0$ state, thus spin state information can be extracted from the fluorescence intensity. Meanwhile, populations in the $^1$A singlet has large probability of jumping back to the $m_S = 0$ ground state, so the off-resonant laser excitation also polarize the electron spin to the $m_S = 0$ state.

### 2.1. Optically detected magnetic resonance (ODMR)

The spin-dependent optical transitions enable room temperature ODMR of an NV center. This technique can be understood in analogy with the electron paramagnetic resonance (EPR) or nuclear magnetic resonance (NMR), while the optical pulses instead of the huge magnetic fields are employed to polarize (and readout) the target spins. As discussed above, a very high spin polarization (> 90%) can be built at room temperature, even in the absence of a large magnetic field.[46–49] Technically, there are two classes of ODMR measurements, continuous-wave (CW) ODMR and pulsed-ODMR.[55] CWODMR spectra are obtained by simultaneously applying laser excitation, fluorescence readout and MW driving of sweeping frequencies. CWODMR has limited frequency resolution (several MHz) due to the power broadening of the laser and MW pulses, but the fast scan speed makes it useful in extracting the resonant frequency of an NV electron spin. Figure 1(d) presents a typical CWODMR spectrum of an NV center under an external magnetic field of 24 Gs (1 Gs = $10^{-4}$ T). In pulsed-ODMR, the MW driving pulses are isolated from the optical polarization and readout process, so much higher spectrum resolution can be obtained and dedicated control sequences can be applied to the target spins, see details in the following sections.

Figure 2 presents the pulse sequence and experimental results of coherent manipulations of an NV electron spin. As

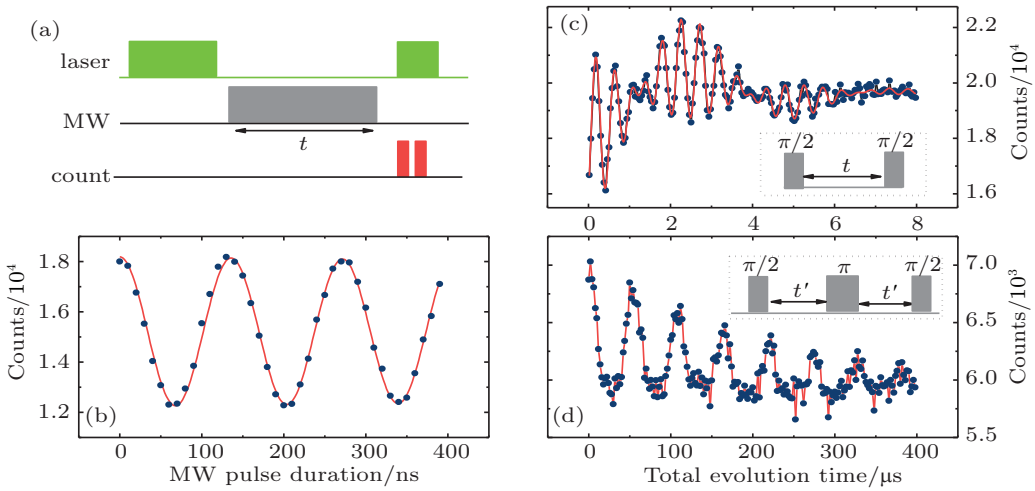



**Fig. 2.** (color online) Coherent manipulation and characterization of a single NV electron spin. (a) Pulse sequence. The first green laser polarize the electron spin to the $m_S = 0$ state, then resonant microwave (MW) pulses are applied to drive the coherent evolution of the electron spin. After manipulation, the spin state is readout by counting the fluorescence intensity. (b) Rabi oscillation of the NV electron spin under resonant driving. The signal is measured with pulse sequence in panel (a). (c) Ramsey fringes (FID) of the NV electron spin. The fast modulation is caused by the host $^{14}$N nuclear spin and the slow modulation is caused by a $^{13}$C nuclear spin. (d) Spin echo (Hahn echo) of the NV electron spin. The collapse and revival behavior is caused by the Larmor precession of its surrounding $^{13}$C nuclear spins. Inset of panels (c) and (d): the used pulse sequence.

shown in Fig. 2(a), the electron spin is first polarized to the $m_S = 0$ state by the short laser pulse (about 3 microseconds), then a resonant MW pulse is applied to drive the Rabi oscillation of this single spin. After that, a second laser pulse is used to readout the spin state, where the population information is recorded by the fluorescent photon counts. Figure 2(b) is a typical Rabi oscillation signal of this single spin. The NV spin state can be flipped in tens of nanosecond, which is very fast compared to its spin coherence time. We also present the coherence measurement results of this NV center in Figs. 2(c) and 2(d), where the free-induction decay (FID) and spin echo (Hahn echo) signal are measured (NV spin coherence is discussed in the next section).

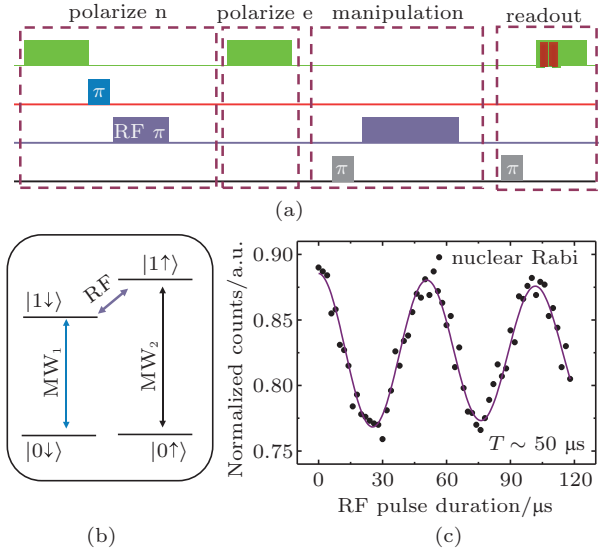



**Fig. 3.** (color online) Coherent manipulation of a single nuclear spin around an NV center. (a) Pulse sequence. A swap gate is employed to polarize and readout the spin state of the nuclear spin. And resonant radiofrequency (RF) pulses are used to manipulate the nuclear spin states. (b) Four-level system composed by the NV electron spin and a strong coupled $^{13}$C nuclear spin. (c) Rabi oscillation of the $^{13}$C nuclear spin, pulse sequence in panel (a) is used.

The spin-dependent optical properties of NV center also enable coherent manipulation of single nuclear spins around an NV center. As shown in Figs. 3(a) and 3(b), by employing the hyperfine interaction between the center electron spin and the nearby $^{13}$C nuclear spins, the optical spin polarization can be transferred onto one of these nuclear spins. Then the target nuclear spin can be manipulated with resonant radiofrequency (RF) pulses, and its final states can be mapped back and readout with the assistance of the same NV center. Figure 3(c) presents typical Rabi oscillation signal of a $^{13}$C nuclear spin, and the typical flip time of a nuclear spin is about tens of microsecond. It is worth noting that the gyromagnetic ratio of nuclear spins is 3 orders smaller than that of electron spins, so the manipulation speed of a nuclear spin is much slower than that of an electron spin. Meanwhile, this difference makes nuclear spins persist much longer coherence time as compared to electron spins.[18,23,24]

### 2.2. Spin relaxation and dephasing

In this section, we discuss the spin coherence of NV centers, which is of crucial importance for all the quantum information processing and quantum sensing applications. The spin state, for example, $|\psi\rangle = \alpha|0\rangle + \beta\, e^{i\phi}|1\rangle$, contains both population and phase information. The process of losing population information is known as longitudinal relaxation, which is caused by the random energy transfer between the center spin and its surrounding environment.[56] At room temperature, a two-phonon Raman process dominates the spin relaxation of NV centers in a characteristic timescale of $T_1$.[57]

The process of losing phase information is known as decoherence (dephasing), which happens in a time scale of $T_2$. For NV centers in diamond, the decoherence is dominated by the hyperfine coupling with its surrounding spins. In type Ib diamond, the large amount of substitutional nitrogen impurities (P1 centers, more than 100 ppm) contribute an electron spin bath and limit $T_2$ to several microseconds.[7] In high-purity IIa diamond (N $<$ 5 ppb), the dominate source of decoherence is the random distributed $^{13}$C nuclear spins, which is about 1.1% in nature abundance, and the typical spin coherence time of NV center in such high-purity diamond is several hundreds of microseconds.[5] Meanwhile, the Larmor precession of the surrounding $^{13}$C nuclear spins contributes a collapse and revival behavior to the center spin coherence signal, as shown in Fig. 2(d).

There is another characteristic time of decoherence named $T_2^*$ in single-spin experiments. As shown in Fig. 2(c), the center electron spin is firstly prepared to the superposition state $(|0\rangle + |1\rangle)/\sqrt{2}$ by an MW $\pi/2$ pulse, then the electron spin will accumulate a phase $\varphi$ determined by the instantaneous magnetic field ($b$) and the evolution duration ($t$), e.g., $\varphi \propto bt$. The final state is $(|0\rangle + e^{i\varphi}|1\rangle)/\sqrt{2}$. A second $\pi/2$ pulse converts the phase information $\varphi$ into population information thus can be measured with fluorescence counts. Due to the limited fluorescence intensity of individual NV centers, the measurement sequence needs to be repeated for more than $10^5$ times to get a good signal to noise ratio (SNR). And there are inevitable (thermal) fluctuations in the magnetic field ($b$), thus the average result of all the repeated trials, which is determined by the thermal distribution of the surrounding $^{13}$C nuclear spins, has much shorter coherent oscillation time.[57] The $T_2^*$ of an NV electron spin in high-purity diamond is about several microseconds.[9,58]

Besides the above mentioned thermal fluctuations, the local field also shows quantum fluctuations, which affects the coherence of the center electron spin. In general, the local field operator $b$ does not commute with the total Hamiltonian of the spin bath $H_E$, thus the eigenstates of the local field will evolve to a superposition states of different eigenstates in a later time, which leads to a random distribution of the following mea-

surement on $b$ and causes quantum fluctuations.[7,9] At room temperature, thermal noise is usually much stronger than the quantum fluctuation, so the depasing process of an NV electron spin is dominated by the thermal fluctuations, which has Gaussian distribution and the envelope of the coherence signal shows Gaussian decay. By tuning the strength of the external magnetic field, the effect of quantum fluctuation can be enhanced and became measurable in experiments.

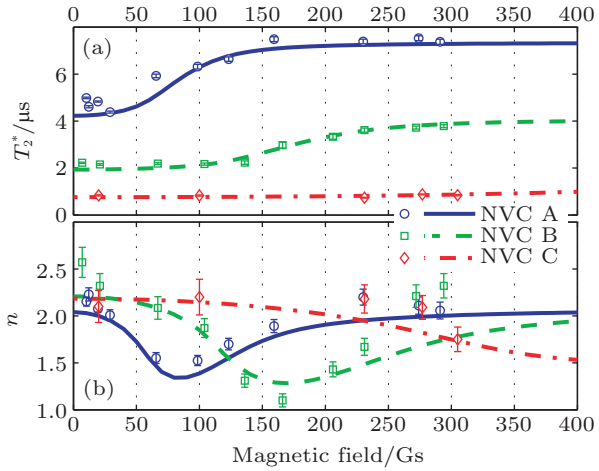



**Fig. 4.** (color online) Controllable effects of quantum fluctuations on the free-induction decay (FID) of an NV center spin: (a) the dephasing time $T_2^*$, and (b) the exponential decay index $n$, for three NV centers (A, B, and C). Experimental data are shown in circle, square, and diamond symbols with error bars, and numerical data are shown in solid, dashed, and dash–dotted lines. By tuning the strength of the external magnetic field, the contribution of quantum fluctuation can be suppressed or enhanced, as evidenced by the vibration of $n$ ($n \neq 2$ represents a non-Gaussian envelop decay, which is a signature of the quantum fluctuation). Reproduced from Ref. [9], NPG.

In Fig. 4, for three different NV centers in high-purity diamond, we present their coherence time $T_2^*$ and decay index $n$ as functions of the external magnetic field strength. The value of $T_2^*$ and $n$ are extracted by fitting the FID signal with the function:

$$S = C\,\mathrm{e}^{-(t/T_2^*)^n}\left[\frac{1}{3}+\frac{2}{3}\cos\left(A_{^{14}\mathrm{N}}t+\phi\right)\right],$$

where $A_{^{14}\mathrm{N}}$ is the hyperfine coupling constant to the $^{14}$N nuclear spin. The index $n$ characterizes the Gaussian ($n = 2$) or non-Gaussian decay behavior of the NV spin coherence, which corresponds to the thermal or quantum fluctuations of the spin bath. It is obviously that all the three NV centers suffer from both quantum and thermal noises. And the competition between those two noises can be controlled by the external magnetic field.[9,58] The extraordinary properties of quantum fluctuation have been investigated in several other works.[7,10,59]

## 3. Protection of center spin coherence

Quantum coherence is fragile but at the core of quantum information processing. In this section, we will discuss two effective strategies, dynamical nuclear spin polarization (DNP) and dynamical decoupling (DD), to combat with the above mentioned noise effects thus protect the coherence of NV-based spin qubits. Furthermore, we will show that DD can be used to selectively address and manipulate nearby weakly coupled $^{13}$C nuclear spins around an NV center, which largely extends the physical resources of scalable quantum computing.

### 3.1. Dynamical nuclear spin polarization (DNP)

The thermal and quantum fluctuations of the unpolarized spin bath cause the decoherence of NV electron spins.[7–9,60] A straight-forward scheme of center spin coherence protection is to polarize the nuclear spin bath and suppress their inhomogeneous broadening, as shown in Fig. 5(a). However, it is usually difficult to establishing significant nuclear spin polarization at room temperature. For NV centers in diamond, their unique spin-dependent optical transitions provide an effective mechanism to polarize the center electron spins. And dynamical nuclear spin polarization (DNP) is the bridge to transfer this spin polarization to the surrounding nuclear spins (spin bath).

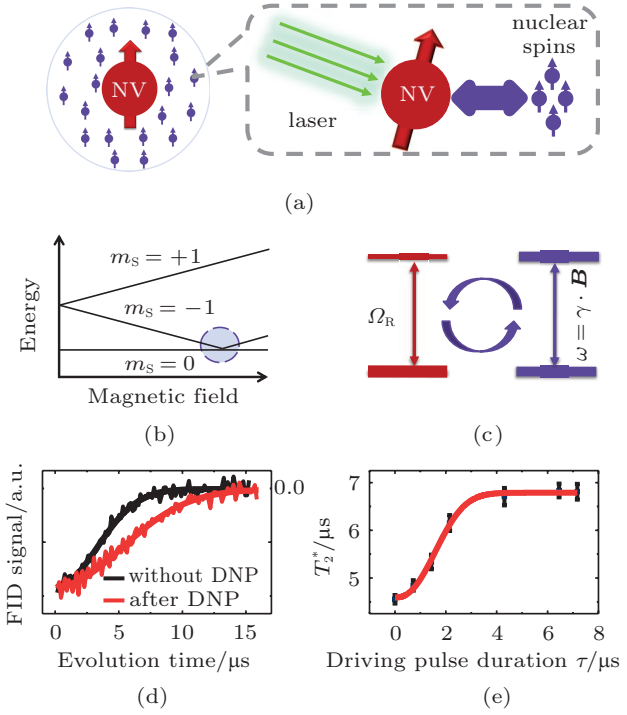



**Fig. 5.** (color online) Protection of center spin coherence by dynamic nuclear spin polarization (DNP). (a) Illustration of the dynamically polarized nuclear spin bath (purple) around an NV center (red). The spin polarization is first built by the green laser pulse, then it can be transfer to the surrounding $^{13}$C nuclear spins under certain conditions. (b) At excited-state level anti-crossing (ESLAC) point, the energy mismatch between the electron spin and nearby nuclear spins is compensated by the external magnetic field (about 500 Gs). (c) The Hartman–Hahn condition. (d) Experimental measured FID signals without (black line) and after (red line) DNP, the prolongation of the dephasing time (from 4.6 μs to 7.4 μs) indicates that the bath spin is polarized during the DNP process. (e) Dependence of the $T_2^*$ time on the DNP pumping duration. Reproduced from Ref. [21], RSC.

The three-order gyromagnetic ratios difference between the electron spin and the nearby nuclear spins blocks the di-

rect polarization transfer between them. Fortunately, with the large zero-field splitting (2.87 GHz for the ground states and 1.4 GHz for the excited states), the energy gap of the electron spin states (between the $m_S = 0$ state and $m_S = -1$ state) is inversely proportional to the strength of the external magnetic field, as shown in Fig. 5(b). And at the level anti-crossing point, there is no energy mismatch between the center electron spin and nearby nuclear spins, thus the spin flip–flop process together with the optical pumping provide an effective channel to polarize the nearby nuclear spins, including the host nitrogen nuclear spin of an NV center.[61]

Under other magnetic fields, the energy mismatch between the two types of spins can be compensated by driving the electron spin (Rabi frequency, in its rotating frame) to the Larmor frequency of the $^{13}$C nuclear spin. This special resonant requirement is known as Hartman–Hahn condition,[62] as shown in Fig. 5(c). Since the spin bath of an NV center contains many $^{13}$C nuclear spins, which are randomly distributed in the diamond lattice and have very different coupling strengths, the polarization transfer process needs to be repeated many circles to build a measurable bath spin polarization. Figure 5(d) presents the FID signals of an NV center with and without DNP, it is clear that the coherence of the center spin can be prolonged with the assistance of DNP. There are many factors affect the final polarization in DNP, including the repeat number, the driving duration under Hartman-Hahn condition, the laser intensity and durations, details can be found in references.[20,21]

### 3.2. Dynamical decoupling (DD)

Dynamical decoupling is a well-developed technique in NMR and ESR,[63,64] and recently it has been demonstrated as an efficient technique to protect the center spin coherence. For NV centers in diamond, there are several nice demonstrations of extending electron spin coherence by DD,[6,19,65] and later on detecting[66–71] and manipulation[29,32,35,37,68,72–74] remote nuclear spins with engineered DD sequence. In this section, we first introduce the working principles of DD-based spin coherence protection, and then discuss the core idea of coherence as a source of quantum sensing. Special attention is paid to the controllable quantum measurement implemented by DD on weakly coupled nuclear spins. A discussion of noise-resilient quantum evolution steered by DD can be found in the section of quantum gate.

#### 3.2.1. Preserving center spin coherence by DD

In the realistic spin bath of an NV center in high-purity diamond, as show in Fig. 6(a), there are many $^{13}$C nuclear spins. They distribute randomly in the diamond lattice, and their hyperfine interactions with the center electron spin are site-dependent. The strongly coupled (closest to the NV center) $^{13}$C nuclear spins can be directly addressed with selective MW pulses[22,23,30,32] and their contribution on the center spin decoherence can be well controlled. For weakly coupled (distant from the NV center) $^{13}$C nuclear spins, they are in large amount but have similar coupling strength to the NV electron spin, thus cannot be distinguished directly in the ODMR spectrum.

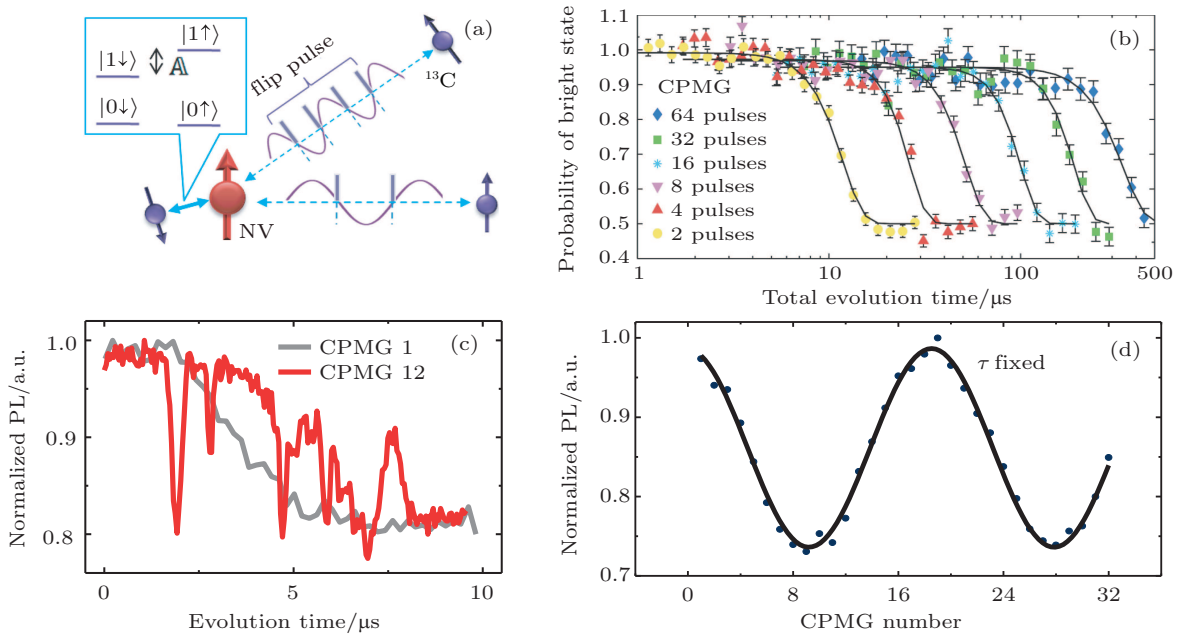



**Fig. 6.** (color online) Protection of center spin coherence by dynamical decoupling (DD). (a) An NV electron spin (red) and its $^{13}$C nuclear spin bath (purple). The spin state of a strongly coupled $^{13}$C nuclear spin can be mapped to the electron spin through selective MW pulses. For weakly coupled nuclear spins, DD is employed to address one of them while decoupling the others. (b) Spin coherence as function of the total evolution time, while CPMG of different pulse numbers is applied. (c) Coherence of the center electron spin under CPMG-12 (red line) and CPMG-1 (gray line), as a function of the pulse interval $\tau$. Different nuclear spins can be selectively addressed by choosing the value of $\tau$. (d) Under the protection of a CPMG sequence, the NV spin state only accumulates a controllable phase from the selected target nuclear spin. Reproduced from Refs. [19] and [29], APS.

Center spin decoherence caused by those weakly coupled nuclear spins can be effectively suppressed with DD sequence. In general, a DD sequence contains many fast-flipping pulses acting on the center electron spin. The bath spin evolution is a quasi-static process compared to the fast flippings, thus the unwanted coupling between the center spin and bath spins can be averaged to zero, and the coherence (phase information of the quantum state) of the center spin can persist for a much longer time under DD sequence.[6,19,65] As shown in Fig. 6(b), a perfect plateau of the coherence signal can be obtained by applying the periodic Carr–Purcell–Meiboom–Gill (CPMG) sequence (one type of DD sequences[19]).

### 3.2.2. Spin coherence and quantum sensing

DD can also be used to amplify the interaction from one selected $^{13}$C nuclear spin and implement controllable quantum measurement on it. This happens when the precession frequency of this nuclear spin matches the flip rate of the DD sequence, thus the phase from this nuclear spin will be added up and the coherence signal of the center spin shows abrupt dips, as shown by the red line in Fig. 6(c). This mechanism provides an easy and effective technique to address those weakly coupled $^{13}$C nuclear spins.[66–69]

After addressing one of the weakly coupled nuclear spins by tuning the pulse intervals, DD can act as a controllable quantum measurement on it. The accumulated phase of the center electron spin from the target nuclear spin is controlled by the pulse number (total interaction time) of the DD sequence (Fig. 6(d)). With a proper phase and an extra rotation on the electron spin, the hybrid system can be prepared to a maximum entanglement states, e.g., $|0\downarrow\rangle+|1\uparrow\rangle$ (see Ref. [29] for details). Then a following projective readout on the electron spin will collapse the state of the nuclear spin simultaneously. By choosing a different pulse number, the target nuclear spin and the center spin can be only partial entangled, then the projective readout on the electron spin corresponds to a weak measurement on the target nuclear spin, in which only partial information of the nuclear spin can be extracted, as shown in Fig. 7(a).

One application of these controllable quantum measurements is to implement single-shot readout of these weakly coupled $^{13}$C nuclear spins, which are good candidates for quantum memories due to their strength in number and good coherence. As discussed in Ref. [29], a set of nuclear spin basis states are stable under repetitively applied DD sequence. As the nuclear spin will be trapped to this state with the repetitively applied DD sequence, and the following projective measurements on the center electron spin give the same results and can be summed up together to extract the state of the target nuclear spin. As shown in Figs. 7(b) and 7(c), with the single-shot readout scheme, quantum jumps of a weakly coupled $^{13}$C nuclear spin are observed under an external magnetic field of 690 Gs at room temperature. This scheme largely extends the range of physical systems for scalable quantum computing.

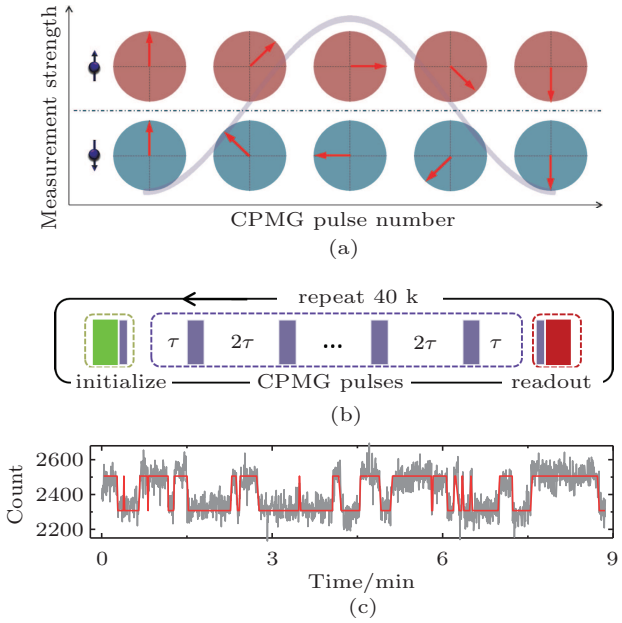



**Fig. 7.** (color online) Controlling the strength of quantum measurements by DD and single-shot readout of a weakly coupled nuclear spin. (a) The accumulated phase of the center electron spin (and thus the measurement strength of the weakly coupled target nuclear spin) is controlled by the pulse number of the applied CPMG sequence. (b) Pulse sequence. The weakly coupled nuclear spin is selectively addressed and its state is mapped to the center electron spin by the CPMG sequence, and then readout by the subsequent projective measurement on the NV electron spin. (c) Typical quantum jump signal of a weakly coupled nuclear spin under an external magnetic field of 691 Gs. Each data point is the sum of $4\times10^4$ trails of the sequence in panel (b). Reproduced from Ref. [29], APS.

## 4. Quantum gate

In quantum computation, a quantum gate is an operation on a few qubits, which manipulates the quantum states to implement elementary tasks. Quantum gates are the building blocks of quantum information processing. In this section, we briefly survey the quantum gates of NV-based spin qubits. The key factors which affect the gate fidelity in experimental implementation, including the pulse imperfections and spin dephasing during manipulation, are discussed.

### 4.1. Plain pulse and shaped pulse

Based on their protocols, these quantum gates can be categorized into four groups, as listed in Table 1. We start with the most simple and direct one, plain pulse. As discussed in the section of ODMR technique, after its polarization, the electron spin of an NV center can be coherently manipulated with a resonant MW pulse. The MW pulse is a segment of electromagnetic waves which can be described by its amplitude, frequency and phase. A resonant MW pulse means the frequency is exactly match the energy gap between the $m_S=0$ and $m_S=\pm1$ states. As depicted in Fig. 8(a), the effect of a quantum gate equals to a rotation of the quantum state on the

**Table 1.** Quantum gates for NV-based spin qubits.

| Schemes | Coherence protection | Robust to pulse errors | Gate speed | Gate fidelity | References |
|---|---|---|---|---|---|
| Plain pulse (MW/RF) | no | no | good | good | [23], [25], [30] |
| Optimal control / Composite pulses[a] | good | good | fast | perfect | [33], [75]–[77] |
| Gate & DD / Gate by DD | good | good | fast | good | [31], [32], [78], [79] |
| Geometric control | — | good | slow | good | [34], [80]–[82] |

[a] In general, only a few of the gate parameters (fidelity, speed, or robustness to pulse errors) are optimized in one of the optimal schemes.

Bloch sphere. The rotating axis is determined by the phase of the MW pulse, and the driving speed is determined by the amplitude of the MW pulse (in rotating frame).

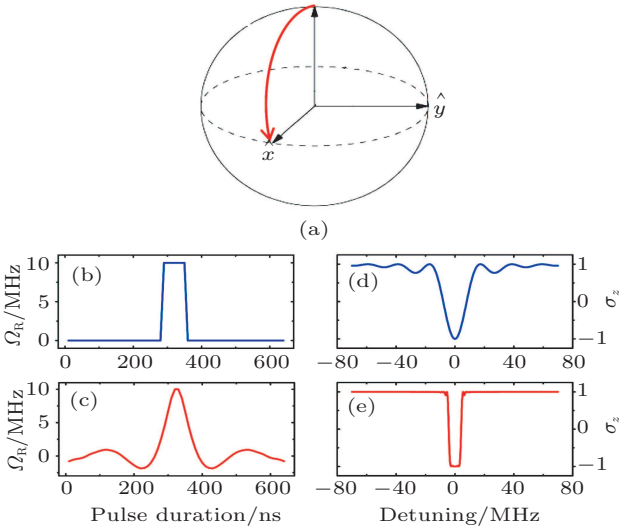



**Fig. 8.** (color online) Quantum gate and its experimental implementation. (a) A single qubit quantum gate (Hadamard gate) can be understood as a rotation on the Bloch sphere. (b) The envelop of a plain pulse and (c) a shaped pulse (REBURP) in the time domain. The carrier frequency is ignored in this schematic plot. Panels (d) and (e) are the same pulses as shown in panels (b) and (c), but in frequency domain. The shaped pulse has almost equal excitation in a sharply edged region, makes it particularly suite for the selective excitations. Reproduced from Ref. [76], AIP.

In realistic experimental implementation, the shape of an MW pulse is important to combat the noise effects. Figure 8(b) presents the shape of a plain pulse (square). Due to its finite duration, which is always true in experiment, the frequency spectrum of this pulse becomes broadened. So this plain pulse may excite other transitions in the adjacent frequency domain (Fig. 8(d)). For an NV center in diamond, the host $^{14}$N and nearby $^{13}$C nuclear spins brings complicated hyperfine structure,[56,84] and this plain pulse may fail in selectively driving only one of the transitions. This problem can be solved by adjusting the shape of the MW pulse, as shown in Fig. 8(c). For the shaped pulse, its sharp edge in the frequency domain (Fig. 8(e)) makes it well suitable for the circumstance of selective excitations.[76] The shaped pulse belongs to a more general category of optimal control, see the following section for more discussion.

### 4.2. High fidelity quantum gates by optimal control

To achieve fault-tolerant quantum control, one needs to analysis the qubit system as well as the applied driving pulses.[84,85] As demonstrated in reference,[33] the gate errors may come from the Overhauser field of an NV center, the magnetic field fluctuation, the instability of the microwave frequency, and pulse distortions due to the above mentioned finite bandwidth, or the instability of the microwave source. These imperfections can be eliminated with dedicated control techniques. For example, the phase and amplitude distortions of an MW pulse can be corrected by the pulse-fixing technique. Furthermore, with the knowledge of the noise sources, one can design composite pulse to combat them. In Ref. [33], a composite pulses named BB1inC has achieved single-qubit gate fidelity of 0.999952(6). Meanwhile, a two-qubit gate with fidelity of 0.992 is implemented by an optimized GRAPE pulses, as shown in Fig. 9. With these high-fidelity quantum gates, it is possible to implement fault-tolerant quantum computation.

### 4.3. Quantum gates with simultaneous effect of coherence protection

The above discussion focuses on either the task of coherence protection or the implementation of quantum gates. It is nature to ask whether there is a scheme to achieve both goals simultaneously. As DD is an effective technique to protect the center spin coherence, a direct solution to this problem is applying both the DD pulses and gate pulses simultaneous. However, this is a non-trivial mission since the two control pulses may distort the effect of each other. Nevertheless, several groups have demonstrated that it is possible to implement the quantum gates while using a DD sequence to protect the center spin coherence.[31,79] These schemes can be classified into the gate while DD (see Table 1 for the comparison between different schemes).

We now introduce another scheme, named as gate by DD, which uses only the DD pulses to achieve both the gate operation and the coherence protection. The essential idea of DD-based nuclear spins manipulation is to fully exploit their electron spin state dependent evolution. Taking a nearby $^{13}$C nuclear spin for example, as shown in Fig. 3(b), the precession axis and frequency of the nuclear spin are determined by both the external magnetic field and the NV electron spin.[7,22,32,37] Since the DD sequence is built with electron spin flips, the trajectory of the nearby $^{13}$C nuclear spin can be completely alternated by the DD sequence.

As shown in Fig. 10(a), in the operator space of the hybrid system, if one lets the initial state to evolve freely, the fast

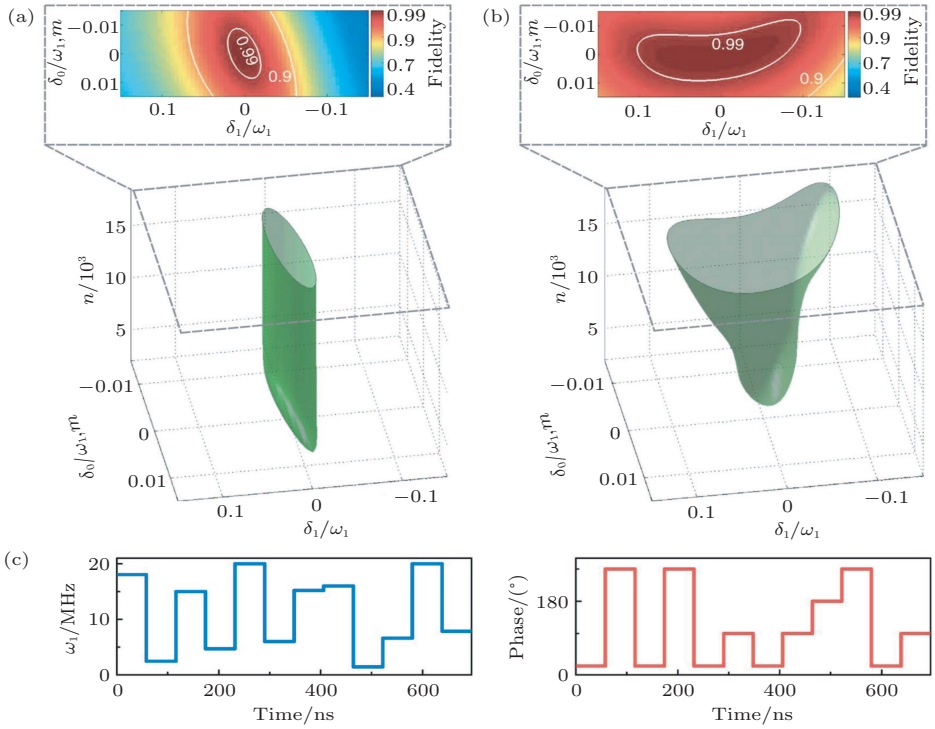



**Fig. 9.** (color online) High fidelity universal quantum gate implemented by optimal composite pulses. (a) and (b) Gate fidelity of an original gradient ascent pulse engineering (GRAPE) (a) and a modified one (b). The upper figures are the contour maps of the gate fidelity. The modified GRAPE is more robust to the noise effects and pulse errors. A CNOT gate with fidelity of 0.992 is achieved with this modified GRAPE. (c) The used pulse parameters of the optimal control experiment. The left (right) one is the amplitude (phase) sequence. Reproduced from Ref. [33], NPG.

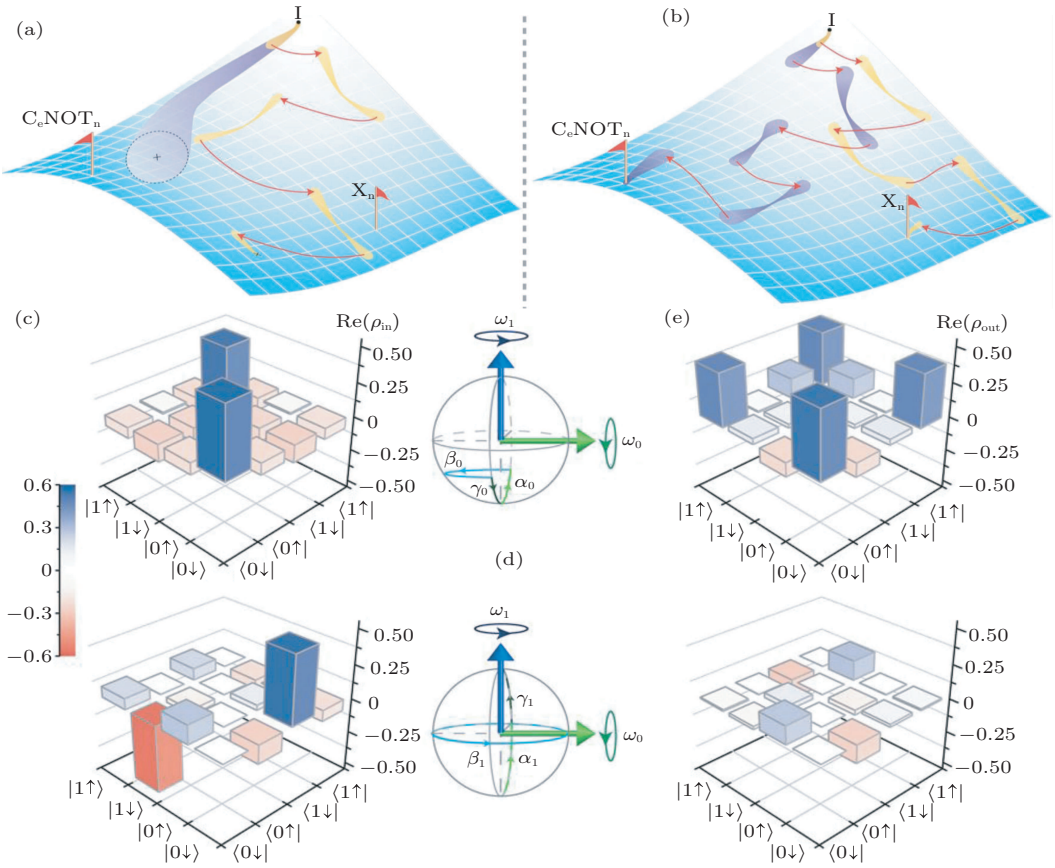



**Fig. 10.** (color online) Noise-resilient quantum gates implemented by DD. (a) Propagator evolution in the conventional settings of FID or periodic CPMG sequence in the operator space. (b) In contrast to the conventional schemes, one can relax the timing constraint in applying the DD pulses and thereby steer the system propagator to the desired points in the operator space. For instance, the C-NOT and the nuclear qubit Pauli-X (Xn) gates can be realized by the purple and the yellow paths, respectively. The gate is characterised by performing state tomography of the two-qubit system before and after its implementation. (c) State tomography for the initial state $|0\downarrow\rangle\sqrt{2}-\mathrm{i}|1\downarrow\rangle$. (d) Schematic diagram of the conditional evolution of the $|0\downarrow\rangle$ (upper panel) and $|1\downarrow\rangle$ (lower panel) states steered by the DD. (e) State tomography of the output Bell state $|0\downarrow\rangle\sqrt{2}+|1\uparrow\rangle$ for the initial state in (c). Reproduced from Ref. [32], NPG.

decoherence of the center electron spin brings large uncertainty to the final state, and the path of the propagator spreads out in the operator space. In a conventional DD sequence, for example, CPMG (yellow path), flipping pulses (red arrows) are applied periodically to protect the coherence of center electron spin, and the uncertainty of the final state is refocused. However, the evolution of the nearby nuclear spin is driven by the flipping of the electron spin, and usually the resultant propagator of the hybrid system under conventional DD sequence is not a target one, e.g., the results of a CNOT gate. With this in mind, one can relax the timing constraint in applying the DD sequence, which can steer the quantum evolution of the nearby $^{13}$C nuclear spin while protect the coherence of the center electron spin. This corresponds to steer the system propagator to a desired point in the operator space, as illustrated in Fig. 10(b).

To demonstrate the DD-steered quantum gate, the coupling strength between a nearby $^{13}$C nuclear spin and the center electron spin is measured in experiment, and then it is used in the numerical simulations of optimizing the effect of the DD sequence, with the aims of preserving the electron spin coherence as well as steering the quantum evolution of the target nuclear spin. Figures 10(c) and 10(d) present the experimental results of a DD-steered CNOT gate on a two-qubit system. FID measurement after the implement of the DD-steered gates shows that the coherence of the center electron spin is well protected during the gate operation, see Ref. [32] for details.

There are other schemes to implement quantum gate on these spin qubits (Table 1). For example, universal holonomic quantum gates have been demonstrated with the NV electron spin and its host $^{14}$N nuclear spin. These geometric approaches may have some built-in noise-resilience features, details can be found in references.[34,80–82]

## 5. Applications of few spin qubits

Although the one or two well-controlled spin qubits are far away from a realistic quantum computer, they provide a good platform to exploit and verify fundamental issues in quantum information processing, such as demonstration of quantum cloning machine,[40,41] quantum error correction,[36,37] quantum Zeno effect,[72,86] and quantum algorithm.[31,34,39,42] In this section, as examples, we discuss the demonstration of entanglement enhanced phase estimation[87] and loophole-free Bell inequality violation.[88]

### 5.1. Enhancement of phase estimation by entanglement

Quantum parameter estimation is the emerging field of yielding higher statistical precision of unknown parameters by harnessing entanglement and other quantum resources. Precise parameter estimation is of crucial importance in science and technology. Repeating measurement is the straightforwards protocol to decease the statistical error in estimation. However, it is not the most efficient strategy. In the case of using $N$ particles to estimate a parameter $\varphi$, if these $N$ particles are independent, the standard quantum limit (SQL) gives the scaling law of the uncertainty on the averaging numbers $\delta\varphi \propto 1/\sqrt{N}$. As a comparison, if one use $N$ entangled particles, in principle the Heisenberg limit scaling $\delta\varphi \propto 1/N$ can be achieved.

A well controlled two-spin system (an NV electron spin and its nearby $^{13}$C nuclear spin) is employed to demonstrate the entanglement-enhanced phase estimation protocol. The phase of the spin qubits is the parameter of interested, which can be prepared and measured with the techniques mentioned in Ref. [87]. The two spin qubits can be prepared and measured independently, as shown in the upper pane of Fig. 11(a). The errors of phase estimation from those two spin qubits follows the scaling law of $\delta\varphi \propto 1/\sqrt{N}$, and the combination of both measurements (independent) gives another enhancement of $1/\sqrt{2}$. As a comparison, the two well-controlled spin qubits can be entangled before the phase estimation process, as shown in the lower pane of Fig. 11(a). In this case, the entanglement makes the two spins sharing their phases, and a total $2\varphi$ phase is extracted from each measurement on them, which gives an enhancement of $1/2$ when the entangled state is fully exploited.

For different repeat number and input phases, the uncertainties of phase estimation with independent and entangled states are compared in Figs. 11(b)–11(d). Figure 11(b) presents the Rabi amplitude as function of the input phases,[87] which is used to estimate the phase information. It is clear that the entangled states have doubled phase dependence as compared to the independent states. In Fig. 11(c), by increasing the repeat number $N$, the scaling law of $\delta\varphi \propto 1/\sqrt{N}$ are obtained for both measurements, and the entangled states always have smaller phase errors compared to the independent states, these measurements are carry out with a phase of 30°. The entanglement enhancement is also verified with other input phases, as shown in Fig. 11(d). It is worth noting that in the current proof-of-principle demonstration, all phases are encoded into the spin qubits by MW or RF pulses, and the decoherence effect of the spin qubits are not take into account since the pulses are much shorter compared to the spin coherence time. However, the much faster decohernce of the entangled states should be taken into account in realistic applications, where in general the phase accumulation process may take a longer duration.[89,90]

### 5.2. Loophole-free Bell inequality violation

Bell's inequality[93] provides an experimental measurable scheme to verify the difference between quantum mechanics and local hidden variables theories. It is of crucial importance in understanding the fundamental property of nature

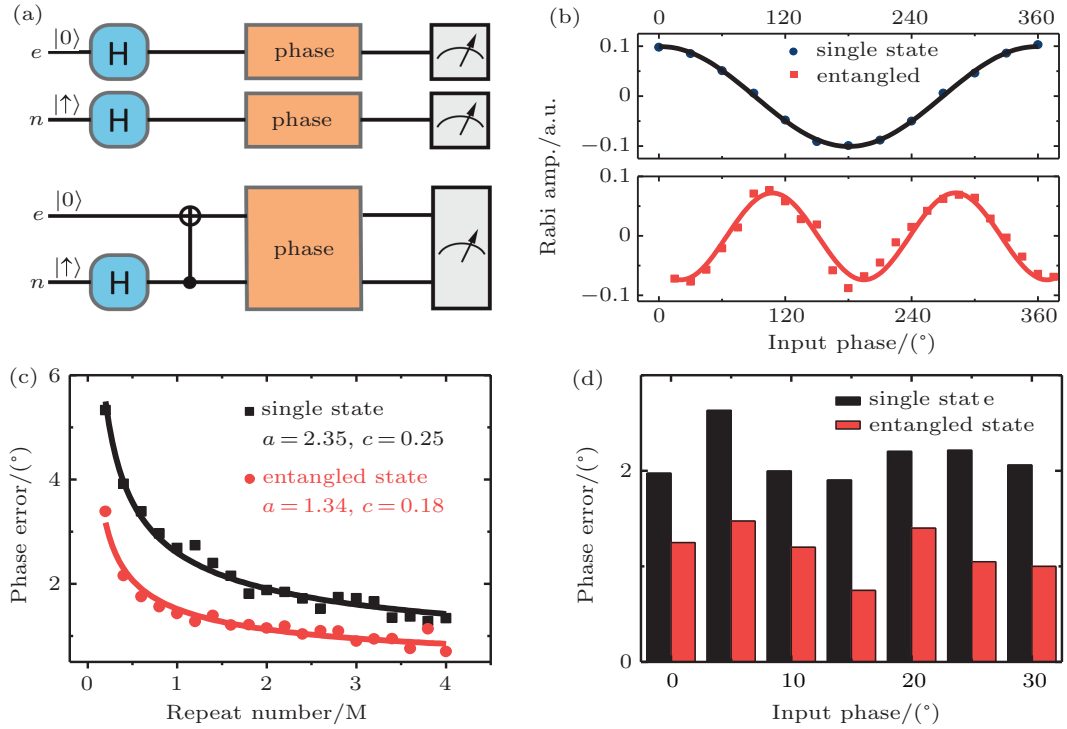



**Fig. 11.** (color online) Entanglement-enhanced phase estimation. (a) Phase estimation schemes of the independent states and the electron-nuclear entangled state. By harnessing entanglement, quantum metrology yields higher statistical precision than classical approaches. (b) Phase relation of an independent states and entangled states. (c) The phase uncertainty is fitted by function $\delta\varphi = a/\sqrt{\nu} + c$ for both single spin state and the entangled state, where $\nu$ corresponds to repeat number in unit of million (M). The curves show that the phase uncertainty, phase error represented by $\delta\varphi$, of entanglement case is apparently lower than the case of single spin state. (d) The phase error of different input phases, the repeat number is fixed to 1 M. Reproduced from Ref. [87], NPG.

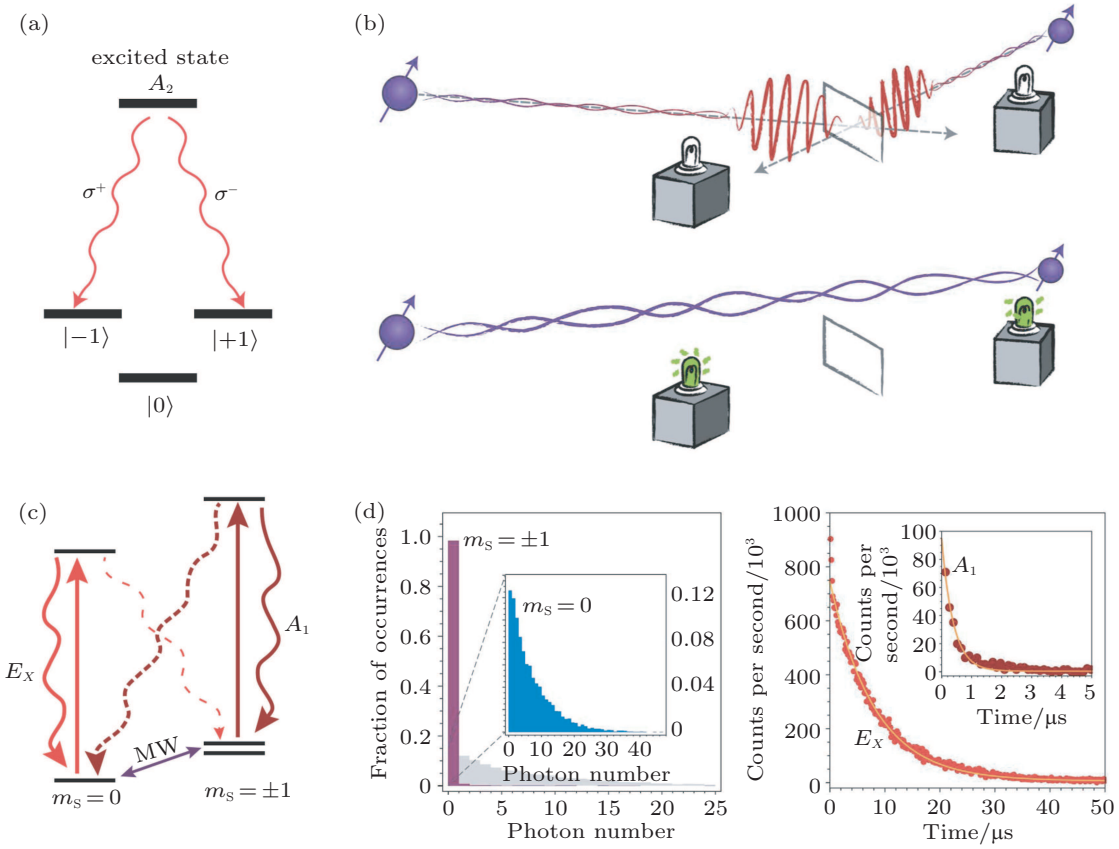



**Fig. 12.** (color online) Elements of the loophole-free Bell inequality violation experiment.[88] (a) The lambda transition makes it is possible to entangle the NV electron spin state with the polarization of an emitted photon. For example, the detection of a $\sigma^+$ photon indicates that the electron spin is at the $m_S = -1$ state.[91] (b) A measurement-based scheme to entangle two remote spins, with the assistance of flying qubits. Adapted from Ref. [92], MRS. (c) Energy levels and (d) typical results of single-shot readout of the NV electron spin state under resonant excitation (left). The spin-selective transitions in panel (c) can be used to polarize the spin state with high fidelity (right). Reproduced from Ref. [27], NPG.

and it is the guarantee of the device-independent quantum cryptography.[94] In this section, we introduce the recent loophole-free Bell inequality violation experiment with NV centers in diamond.

Bell's inequality can be verified with entangled particles, as proposed in reference.[95] There are two major loopholes in all the Bell test experiments: the locality loophole[96] and the detection loophole.[97] To exclude the locality loophole, the entangled particles can be separated far away from each other thus the communication between them during the measurement time is impossible (information can not be transferred faster than light). One candidate for such demonstration is entangled photon pairs.[98] However, these flying qubits always suffer from the photon loss during the spatial distribution of entanglement and also the imperfection in detection, which lead to the detection loophole.

In the NV-based Bell inequality experiment,[88] both of the loopholes are excluded. The locality loophole is excluded by establishing remote entanglement of two NV electron spins (1.3 km). As shown in Figs. 12(a) and 12(b), the states of photons emitted from an NV center are correlated with the final spin states. With an measurement-based protocol, the two remote electron spins can be entangled.[99,100] The 1.3-km distance between the two spins gives a time window of 4.27 μs, which is longer enough to implement the single-shot readout scheme (3.7 μs is used in the experiment). The single-shot readout scheme is employed to excluded the detection loophole, which means every entangled spin state is measured with high fidelity. Figures 12(c) and 12(d) show the energy levels and typical results of single-shot readout, where resonant optical excitation of an NV electron spin is employed, see Ref. [27] for details.

The statistic of 245 trials of CHSH–Bell inequality give $S = 2.426 \pm 0.20$, which is a solid evidence of Bell inequality violation (CHSH–Bell inequality states $S \leq 2$, where $S$ quantifies the correlation between measurement outcomes).[88] Another repeat experiment gives similar results and pushes the overall value to $S = 2.38 \pm 0.14$.[101] There is another NV-based Bell test experiment, shows that a temporal Bell Inequality is violated.[102] It is clear that NV centers in diamond is an excellent test-bed system to exploit and understand the nature.

## 6. Conclusion and perspectives

In summary, we discussed the basic properties and experimental techniques to manipulate the NV spin qubits. These qubits include the electron spin of an NV center and the nearby nuclear spins. The randomly distributed nuclear spins are the sources of the electron spin decoherence, but they also could be a good resources of multi-qubit system.

With dynamical nuclear spin polarization, the coherence of center electron spins can be prolonged, and this technique can be extended to other spins, either inside or outside the diamond lattice, to build a hyperpolarization of surrounding spins, which may benefit the field of NMR and MRI (magnetic resonance imaging). With dynamical decoupling, the nearby nuclear spin can be selectively addressed, manipulated and measured, which offers a great chance in building multi-qubits quantum node (see discussion below), as the elementary part of a quantum repeater and quantum computer. With those well-controlled few spins, we are able to demonstrate and verify fundamental issues in quantum information process, such as entanglement-enhanced phase estimation and loophole-free Bell inequality violation.

At the end of this review, we discuss the strategies of scaling up NV-based qubits for quantum computing and distributed quantum networks.

The straight-forward scheme of scaling up is to couple NV centers with their direct interactions. As demonstrated in reference Ref. [103], when two NV centers are close to each other, for example, with a distance below 10 nm, the coupling between them is strong enough to be observed directly in the CWODMR spectrum. And selective addressing and manipulation are available for those strong coupled NV electron spins. Furthermore, nearby nuclear spins around the NV centers can be harnessed to prolong the lifetime of the spin entanglement.[104] Unfortunately, the deterministic fabrication of directly coupled NV centers, which requires three-dimensional precision better than 10 nm, is still beyond the current techniques.[105–108]

A substantial effort has been geared towards coupling NV electron spin to other solid state quantum systems such as superconducting qubits[109–112] and mechanism resonator.[113–117] In these schemes, the merits of different physical system could be merged together. For example, the convenience in sample fabrication and fast manipulation of superconducting qubits, together with the long coherence time of NV spin ensemble, make such hybrid system as one of the most promising node for scalable quantum computing.[118]

There are also exciting progress in scaling up NV spin qubit with photons. The spin states of NV centers are initialized and readout with optical pulses, and both the excitation and emission photons can be exploited to establish entanglement with the NV electron spins.[24,91] By employing one of the optical lambda transition, Harvard group demonstrated that the polarization of the emission photons preserve good entanglement with the NV spin states.[91] Later, indistinguishable photon emission from two separate NV centers was demonstrated by Delft and Harvard groups, where the optical transition energies difference was compensated by the

dc Stark effect.[99,100] Then Delft group demonstrated remote spin entanglement with a joint measurement on the NV emission photons,[119] which enabled the loophole-free Bell inequality verification[88] and entanglement distillation between solid-state quantum network nodes.[38]

To build a realistic quantum networks or scalable quantum computing with NV centers, quantum nodes with better optical coupling efficiency and longer build-in quantum memory are needed,[120–122] which could be achieved by fabricating photonic nanostructures[123–126] and exploiting the long coherence time of nearby nuclear spins.[24,72,74,127–130] Again, the development of NV-based quantum computing involves cross-disciplinary efforts, and will offer unprecedented rewards in a broad range of frontier studies, such as condensed matter physics and nanoscale magnetic resonance imaging.[45,50,52–54]

## References


[1] Aharonovich I, Castelletto S, Simpson D, Su C, Greentree A and Prawer S 2011 *Rep. Prog. Phys.* **74** 076501
[2] Gruber A, Drabenstedt A, Tietz C, Fleury L, Wrachtrup J and Borczyskowski C 1997 *Science* **276** 2012
[3] Gaebel T, Domhan M, Popa I, Wittmann C, Neumann P, Jelezko F, Rabeau J R, Stavrias N, Greentree AD, Prawer S and Meijer J 2006 *Nat. Phys.* **2** 408
[4] Epstein R, Mendoza F, Kato Y and Awschalom D 2005 *Nat. Phys.* **1** 94
[5] Childress L, Dutt M G, Taylor J, Zibrov A, Jelezko F, Wrachtrup J, Hemmer P and Lukin M 2006 *Science* **314** 281
[6] Hanson R, Dobrovitski V, Feiguin A, Gywat O and Awschalom D 2008 *Science* **320** 352
[7] Zhao N, Ho S W and Liu R B 2012 *Phys. Rev. B* **85** 115303
[8] Maze J R, Taylor J M and Lukin M D 2008 *Phys. Rev. B* **78** 094303
[9] Liu G Q, Pan X Y, Jiang Z F, Zhao N and Liu R B 2012 *Sci. Rep.* **2** 432
[10] Huang P, Kong X, Zhao N, Shi F Z, Wang P F, Liu R B and Du J F 2011 *Nat. Commun.* **2** 570
[11] Yang W, Ma W L and Liu R B 2016 *Rep. Prog. Phys.* **80** 016001
[12] Wang J F, Zhang W L, Zhang J, You J, Li Y, Guo G P, Feng F P, Song X R, Lou L R, Zhu W and Wang G Z 2016 *Nanoscale* **8** 5780
[13] Waldherr G, Beck J, Steiner M, Neumann P, Gali A, Frauenheim T, Jelezko F and Wrachtrup J 2011 *Phys. Rev. Lett.* **106** 157601
[14] Grotz B, Hauf M V, Dankerl M, Naydenov B, Pezzagna S, Meijer J, Jelezko F, Wrachtrup J, Stutzmann M, Reinhard F and Garrido J A 2012 *Nat. Commun.* **3** 729
[15] Beha K, Batalov A, Manson N B, Bratschitsch R and Leitenstorfer A 2012 *Phys. Rev. Lett.* **109** 097404
[16] Chen X D, Zou C L, Sun F W and Guo G C 2013 *Appl. Phys. Lett.* **103** 013112
[17] Balasubramanian G, Neumann P, Twitchen D, Markham M, Kolesov R, Mizuochi N, Isoya J, Achard J, Beck J, Tissler J, Jacques V, Hemmer P R, Jelezko F and Wrachtrup J 2009 *Nat. Mater.* **8** 383
[18] Maurer P C, Kucsko G, Latta C, Jiang L, Yao N Y, Bennett S D, Pastawski F, Hunger D, Chisholm N, Markham M, Twitchen D J, Cirac J I and Lukin M D 2012 *Science* **336** 1283
[19] Ryan C A, Hodges J S and Cory D G 2010 *Phys. Rev. Lett.* **105** 200402
[20] London P, Scheuer J, Cai J M, Schwarz I, Retzker A, Plenio M B, Katagiri M, Teraji T, Koizumi S, Isoya J, Fischer R. McGuinness L P, Naydenov B and Jelezko F 2013 *Phys. Rev. Lett.* **111** 067601
[21] Liu G Q, Jiang Q Q, Chang Y C, Liu D Q, Li W X, Gu C Z, Po H C, Zhang W X, Zhao N and Pan X Y 2014 *Nanoscale* **6** 10134
[22] Dutt M G, Childress L, Jiang L, Togan E, Maze J, Jelezko F, Zibrov A S, Hemmer P R and Lukin M D 2007 *Science* **316** 1312
[23] Jiang L, Hodges J S, Maze J R, Maurer P, Taylor J M, Cory D G, Hemmer P R, Walsworth R L, Yacoby A, Zibrov A S and Lukin M D 2009 *Science* **326** 267
[24] Yang S, Wang Y, Rao D B, Tran T H, Momenzadeh A S, Markham M, Twitchen D J, Wang P, Yang W, Stöhr R, Neumann P, Kosaka H and Wrachtrup J 2016 *Nat. Photon.* **10** 507
[25] Neumann P, Mizuochi N, Rempp F, Hemmer P, Watanabe H, Yamasaki S, Jacques V, Gaebel T, Jelezko F and Wrachtrup J 2008 *Science* **320** 1326
[26] Neumann P, Beck J, Steiner M, Rempp F, Fedder H, Hemmer P R, Wrachtrup J and Jelezko F 2009 *Science* **329** 542
[27] Robledo L, Childress L, Bernien H, Hensen B, Alkemade P F and Hanson R 2011 *Nature* **477** 574
[28] Dréau A, Spinicelli P, Maze J R, Roch J F and Jacques V 2013 *Phys. Rev. Lett.* **110** 060502
[29] Liu G Q, Xing J, Ma W L, Wang P, Li C H, Po H C, Zhang Y R, Fan H, Liu R B and Pan X Y 2017 *Phys. Rev. Lett.* **118** 150504
[30] Jelezko F, Gaebel T, Popa I, Domhan M, Gruber A and Wrachtrup J 2004 *Phys. Rev. Lett.* **93** 130501
[31] Van der Sar T, Wang Z H, Blok M S, Bernien H, Taminiau T H, Toyli D M, Lidar D A, Awschalom D D, Hanson R and Dobrovitski V V 2012 *Nature* **484** 82
[32] Liu G Q, Po H C, Du J, Liu R B and Pan X Y 2013 *Nat. Commun.* **4** 2254
[33] Rong X, Geng J P, Shi F Z, Liu Y, Xu K B, Ma W C, Kong F, Jiang Z, Wu Y and Du J F 2015 *Nat. Commun.* **6** 8748
[34] Zu C, Wang W B, He L, Zhang W G, Dai C Y, Wang F and Duan L M 2014 *Nature* **514** 72
[35] Casanova J, Wang Z Y and Plenio M B 2016 *Phys. Rev. Lett.* **117** 130502
[36] Waldherr G, Wang Y, Zaiser S, Jamali M, Schulte-Herbrüggen T, Abe H, Ohshima T, Isoya J, Du J F, Neumann P and Wrachtrup J 2014 *Nature* **506** 204
[37] Taminiau T H, Cramer J, van der Sar T, Dobrovitski V V and Hanson R 2014 *Nat. Nanotech.* **9** 171
[38] Kalb N, Reiserer A A, Humphreys P C, Bakermans J J, Kamerling S J, Nickerson N H, Benjamin S C, Twitchen D J, Markham M and Hanson R 2017 *Science* **356** 928
[39] Shi F Z, Rong X, Xu N Y, Wang Y, Wu J, Chong B, Peng X H, Kniepert J, Schoenfeld R S, Harneit W, Feng M and Du J F 2010 *Phys. Rev. Lett.* **105** 040504
[40] Chang Y C, Liu G Q, Liu D Q, Fan H and Pan X Y 2013 *Sci. Rep.* **3** 1498
[41] Pan X Y, Liu G Q, Yang L L and Fan H 2011 *Appl. Phys. Lett.* **99** 051113
[42] Xu K B, Xie T Y, Li Z K, Xu X K, Wang M Q, Ye X Y, Kong F, Geng J P, Duan C K, Shi F Z and Du J F 2017 *Phys. Rev. Lett.* **118** 130504
[43] Maze J R, Stanwix P L, Hodges J S, Hong S, Taylor J M, Cappellaro P, Jiang L, Dutt M G, Togan E, Zibrov A S and Yacoby A 2008 *Nature* **455** 644
[44] Balasubramanian G, Chan I Y, Kolesov R, Al-Hmoud M, Tisler J, Shin C, Kim C, Wojcik A, Hemmer P R, Krueger A, Hanke T, Leitenstorfer A, Bratschitsch R, Jelezko F and Wrachtrup J 2008 *Nature* **455** 648
[45] Degen C L, Reinhard F and Cappellaro P 2017 *Rev. Mod. Phys.* **89** 035002
[46] Jelezko F and Wrachtrup J 2006 *Phys. Status Solidi A* **203** 3207
[47] Dobrovitski V V, Fuchs G D, Falk A L, Santori C and Awschalom D D 2013 *Ann. Rev. Condens. Matter Phys.* **4** 23
[48] Doherty M W, Manson N B, Delaney P, Jelezko F, Wrachtrup J and Hollenberg L C 2013 *Phys. Rep.* **528** 1
[49] Acosta V and Hemmer P 2013 *MRS Bull.* **38** 127
[50] Schirhagl R, Chang K, Loretz M and Degen C L 2014 *Ann. Rev. Phys. Chem.* **65** 83
[51] Rondin L, Tetienne J P, Hingant T, Roch J F, Maletinsky P and Jacques V 2014 *Rep. Prog. Phys.* **77** 056503
[52] Zhou J W, Wang P F, Shi F Z, Huang P, Kong X, Xu X K, Zhang Q, Wang Z X, Rong X and Du J F 2014 *Front. Phys.* **9** 587
[53] Suter D and Jelezko F 2016 *Prog. Nucl. Magn. Reson. Spectros.* **98** 50
[54] Hui Y Y, Cheng C A, Chen O Y and Chang H C 2016 *Carbon Nanoparticles and Nanostructures* (Springer International Publishing) pp. 109–137)
[55] Dréau A, Lesik M, Rondin L, Spinicelli P, Arcizet O, Roch J F and Jacques V 2011 *Phys. Rev. B* **84** 195204
[56] Ladd T D, Jelezko F, Laflamme R, Nakamura Y, Monroe C and O'Brien J L 2010 *Nature* **464** 45
[57] Jarmola A, Acosta V M, Jensen K, Chemerisov S and Budker D 2012 *Phys. Rev. Lett.* **108** 197601

[58] Maze J R, Dréau A, Waselowski V, Duarte H, Roch J F and Jacques V 2012 *New J. Phys.* **14** 103041
[59] Reinhard F, Shi F, Zhao N, Rempp F, Naydenov B, Meijer J, Hall L T, Hollenberg L, Du J F, Liu R B and Wrachtrup J 2012 *Phys. Rev. Lett.* **108** 200402
[60] Hanson R, Gywat O and Awschalom D D 2006 *Phys. Rev. B* **74** 161203
[61] Jacques V, Neumann P, Beck J, Markham M, Twitchen D, Meijer J, Kaiser F, Balasubramanian G, Jelezko F and Wrachtrup J 2009 *Phys. Rev. Lett.* **102** 057403
[62] Hartmann S and Hahn E 1962 *Phys. Rev.* **128** 2042
[63] Carr H Y and Purcell E M 1954 *Phys. Rev.* **94** 630
[64] Meiboom S and Gill D 1958 *Rev. Sci. Instrum.* **29** 688
[65] Naydenov B, Dolde F, Hall L T, Shin C, Fedder H, Hollenberg L C, Jelezko F and Wrachtrup J 2011 *Phys. Rev. B* **83** 081201
[66] Zhao N, Hu J L, Ho S W, Wan J T and Liu R B 2012 *Nat. Nanotech.* **6** 242
[67] Zhao N, Honert J, Schmid B, Klas M, Isoya J, Markham M, Twitchen D, Jelezko F, Liu R B, Fedder H and Wrachtrup J 2013 *Nat. Nanotech.* **7** 657
[68] Taminiau T H, Wagenaar J J, Van der Sar T, Jelezko F, Dobrovitski V V and Hanson R 2012 *Phys. Rev. Lett.* **109** 137602
[69] Kolkowitz S, Unterreithmeier Q P, Bennett S D and Lukin M D 2012 *Phys. Rev. Lett.* **109** 137601
[70] Shi F Z, Kong X, Wang P F, Kong F, Zhao N, Liu R B and Du J F 2014 *Nat. Phys.* **10** 21
[71] Ma W L and Liu R B 2016 *Phys. Rev. Appl.* **6** 024019
[72] Kalb N, Cramer J, Twitchen D J, Markham M, Hanson R and Taminiau T H 2016 *Nat. Commun.* **7** 13111
[73] Cramer J, Kalb N, Rol M A, Hensen B, Blok M S, Markham M, Twitchen D J, Hanson R and Taminiau T H 2016 *Nat. Commun.* **7** 11526
[74] Reiserer A, Kalb N, Blok M S, van Bemmelen K J, Taminiau T H, Hanson R, Twitchen D J and Markham M 2016 *Phys. Rev. X* **6** 021040
[75] Dolde F, Bergholm V, Wang Y, Jakobi I, Naydenov B, Pezzagna S, Meijer J, Jelezko F, Neumann P, Schulte-herbrüggen T, Biamonte J and Wrachtrup J 2014 *Nat. Commun.* **5** 3371
[76] Chang Y C, Xing J, Zhang F H, Liu G Q, Jiang Q Q, Li W X, Gu C Z, Long G L and Pan X Y 2014 *Appl. Phys. Lett.* **104** 262403
[77] Geng J P, Wu Y, Wang X T, Xu K B, Shi F Z, Xie Y J, Rong X and Du J F 2016 *Phys. Rev. Lett.* **117** 170501
[78] Rong X, Geng J P, Wang Z X, Zhang Q, Ju C Y, Shi F Z, Duan C K and Du J F 2014 *Phys. Rev. Lett.* **112** 050503
[79] Zhang J and Suter D 2015 *Phys. Rev. Lett.* **115** 110502
[80] Arroyo-Camejo S, Lazariev A, Hell S W and Balasubramanian G 2014 *Nat. Commun.* **5** 4870
[81] Zhou B B, Jerger P C, Shkolnikov V O, Heremans F J, Burkard G and Awschalom D D 2017 *Phys. Rev. Lett.* **119** 140503
[82] Sekiguchi Y, Niikura N, Kuroiwa R, Kano H and Kosaka H 2017 *Nat. Photon.* **11** 309
[83] Smeltzer B, Childress L and Gali A 2011 *New J. Phys.* **13** 025021
[84] Wang P F, Yuan Z H, Huang P, Rong X, Wang M Q, Xu X K, Duan C K, Ju C Y, Shi F Z and Du J F 2015 *Nat. Commun.* **6** 6631
[85] Liu Y, Kong F, Shi F Z and Du J F 2016 *Sci. Bull.* **61** 1132
[86] Qiu J, Wang Y Y, Yin Z Q, Zhang M, Ai Q and Deng F G 2015 *Sci. Rep.* **5** 17615
[87] Liu G Q, Zhang Y R, Chang Y C, Yue J D, Fan H and Pan X Y 2015 *Nat. Commun.* **6** 6726
[88] Hensen B, Bernien H, Dréau A E, Reiserer A, Kalb N, Blok M S, Ruitenberg J, Vermeulen R F, Schouten R N, Abellán C, Amaya W, Pruneri V, Mitchell M W, Markham M, Twitchen D J, Elkouss D, Wehner S, Taminiau T H and Hanson R 2015 *Nature* **526** 682
[89] Escher B, de Matos Filho R and Davidovich R 2011 *Nat. Phys.* **7** 406
[90] Yue J D, Zhang Y R and Fan H 2014 *Sci. Rep.* **4** 5933
[91] Togan E, Chu Y, Trifonov A S, Jiang L, Maze J, Childress L, Dutt M G, Sørensen A S, Hemmer P R, Zibrov A S and Lukin M D 2010 *Nature* **466** 730
[92] Childress L and Hanson R 2013 *MRS Bull.* **38** 134
[93] Bell J S 1964 *Physics* **1** 195
[94] Accín A, Brunner N, Gisin N, Massar S, Pironio S and Scarani V 2007 *Phys. Rev. Lett.* **98** 230501
[95] Clauser J F, Horne M A, Shimony A and Holt R A 1969 *Phys. Rev. Lett.* **23** 880
[96] Brunner N, Cavalcanti D, Pironio S, Scarani V and Wehner S 2014 *Rev. Mod. Phys.* **86** 419
[97] Garg A and Mermin N D 1987 *Phys. Rev. D* **35** 3831
[98] Weihs G, Jennewein T, Simon C, Weinfurter H and Zeilinger A 1998 *Phys. Rev. Lett.* **81** 5039
[99] Bernien H, Childress L, Robledo L, Markham M, Twitchen D and Hanson R 2012 *Phys. Rev. Lett.* **108** 043604
[100] Sipahigil A, Goldman M L, Togan E, Chu Y, Markham M, Twitchen D J, Zibrov A S, Kubanek A and Lukin M D 2012 *Phys. Rev. Lett.* **108** 143601
[101] Hensen B, Kalb N, Blok M S, Dréau A E, Reiserer A, Vermeulen R F, Schouten R N, Markham M, Twitchen D J, Goodenough K and Elkouss D 2016 *Sci. Rep.* **6** 30289
[102] Waldherr G, Neumann P, Huelga S F, Jelezko F and Wrachtrup J 2011 *Phys. Rev. Lett.* **107** 090401
[103] Neumann P, Kolesov R, Naydenov B, Beck J, Rempp F, Steiner M, Jacques V, Balasubramanian G, Markham M L, Twitchen D J, Pezzagna S, Meijer J, Twamley J, Jelezko F and Wrachtrup J 2010 *Nat. Phys.* **6** 249
[104] Dolde F, Jakobi I, Naydenov B, Zhao N, Pezzagna S, Trautmann C, Meijer J, Neumann P, Jelezko F and Wrachtrup J 2013 *Nat. Phys.* **9** 139
[105] Liu Y, Chen G X, Song M, Ci X T, Wu B T, Wu E and Zeng H P 2013 *Opt. Express* **21** 12843
[106] Chen Y C, Salter P S, Knauer S, Weng L, Frangeskou A C, Stephen C J, Ishmael S N, Dolan P R, Johnson S, Green B L and Morley G W 2016 *Nat. Photon.* **11** 77
[107] McLellan C A, Myers B A, Kraemer S, Ohno K, Awschalom D D and Bleszynski Jayich A C 2016 *Nano Lett.* **16** 2450
[108] Scarabelli D, Trusheim M, Gaathon O, Englund D and Wind S J 2016 *Nano Lett.* **16** 4982
[109] Zhu X B, Saito S, Kemp A, Kakuyanagi K, Karimoto S I, Nakano H, Munro W J, Tokura Y, Everitt M S, Nemoto K and Kasu M 2011 *Nature* **478** 221
[110] Kubo Y, Grezes C, Dewes A, Umeda T, Isoya J, Sumiya H, Morishita N, Abe H, Onoda S, Ohshima T and Jacques V 2011 *Phys. Rev. Lett.* **107** 220501
[111] Song W L, Yin Z Q, Yang W L, Zhu X B, Zhou F and Feng M 2015 *Sci. Rep.* **5** 7755
[112] Zheng Y R, Xing J, Chang Y C, Yan Z G, Deng H, Wu Y L, Lü L, Pan X Y, Zhu X B and Zheng D N 2017 *Chin. Phys. B* **26** 020305
[113] Hong S, Grinolds M S, Maletinsky P, Walsworth R L, Lukin M D and Yacoby A 2012 *Nano Lett.* **12** 3920
[114] Kolkowitz S, Jayich A C, Unterreithmeier Q P, Bennett S D, Rabl P, Harris J G and Lukin M D 2012 *Science* **335** 1603
[115] MacQuarrie E R, Gosavi T A, Jungwirth N R, Bhave S A and Fuchs G D 2013 *Phys. Rev. Lett.* **111** 227602
[116] Chen Q, Xu Z Y and Feng M 2010 *Phys. Rev. A* **82** 014302
[117] Cai K, Wang R X, Yin Z Q and Long G L 2017 *Sci. China-Phys. Mech. Astron.* **60** 070311
[118] Kurizki G, Bertet P, Kubo Y, Mølmer K, Petrosyan D, Rabl P and Schmiedmayer J 2015 *Proc. Natl. Acad. Sci.* **112** 3866
[119] Bernien H, Hensen B, Pfaff W, Koolstra G, Blok M S, Robledo L, Taminiau T H, Markham M, Twitchen D J, Childress L and Hanson R 2013 *Nature* **497** 86
[120] Nemoto K, Trupke M, Devitt S J, Stephens A M, Scharfenberger B, Buczak K, Nöbauer T, Everitt M S, Schmiedmayer J and Munro W J 2014 *Phys. Rev. X* **4** 031022
[121] Johnson S, Dolan P R and Smith J M 2017 *Prog. Quantum Electron.* **55** 129
[122] van Dam S B, Humphreys P C, Rozpedek F, Wehner S and Hanson R 2017 *Quantum Sci. Technol.* **2** 034002
[123] Schröder T, Mouradian S L, Zheng J, Trusheim M E, Walsh M, Chen E H, Li L, Bayn I and Englund D 2016 *J. Opt. Soc. Am.* **33** B65
[124] Bogdanović S, van Dam S B, Bonato C, Coenen L C, Zwerver A M, Hensen B, Liddy M S, Fink T, Reiserer A, Lončar M and Hanson R 2017 *Appl. Phys. Lett.* **110** 171103
[125] Jiang Q Q, Liu D Q, Liu G Q, Chang Y C, Li W X, Pan X Y and Gu C Z 2014 *J. Appl. Phys.* **116** 044308
[126] Jiang Q Q, Li W X, Tang C C, Chang Y C, Hao T T, Pan X Y, Ye H T, Li J J and Gu C Z 2016 *Chin. Phys. B* **25** 118105
[127] Wang Z Y, Casanova J and Plenio M B 2017 *Nat. Commun.* **8** 14660
[128] Dong L H, Rong X, Geng J P, Shi F Z, Li Z K, Duan C K and Du J F 2017 *Phys. Rev. B* **96** 205149
[129] Wang W B, Chang X Y, Wang F, Hou P Y, Huang Y Y, Zhang W G, Ouyang X L, Huang X Z, Zhang Z Y, He L and Duan L M 2017 arXiv: 1711.10101v1 [quant-ph]
[130] Perlin M A, Wang Z Y, Casanova J and Plenio M B 2017 arXiv: 1708.09414v1 [quant-ph]